Emergent Fractal Energy Landscape as the Origin of Stress-Accelerated Dynamics in Amorphous Solids

Chaoyi Liu and Yue Fan*
Department of Mechanical Engineering, University of Michigan, Ann Arbor, Michigan 48109, USA

(Received 9 April 2021; revised 23 August 2021; accepted 5 October 2021; published 16 November 2021)

The ageing dynamics in a multiplicity of metastable glasses are investigated at various thermomechanical conditions. By using data analytics to deconvolute the integral effects of environmental factors (e.g., energy level, temperature, stress), and by directly scrutinizing the minimum energy pathways for local excitations, we demonstrate external shear would make the system's energy landscape surprisingly fractal and create an emergent low-barrier mode with highly tortuous pathways, leading to an accelerated relaxation. This finding marks a departure from the classic picture of shear-induced simple bias of energy landscape. The insights and implications of this study are also discussed.

DOI: 10.1103/PhysRevLett.127.215502

Many important properties of amorphous solids, including their deformation, diffusion, ageing, glass transition, etc., are originated from local structural excitations (LSEs), namely, the collective rearrangements of small groups of atoms [1–4]. Given the nature of disordered atomic packings, wide distributions for both LSEs and their associated activation barriers are expected. However, it is difficult to measure the whole spectra in experiments, because existing techniques [5–8] can only provide one or a narrow range of effective activation barriers. Therefore, atomistic modeling has been regarded as a unique tool in unraveling the underlying physics of glasses. While the behaviors of LSEs under stress-driven limit (e.g., athermal quasistatic [9,10] or high strain rates [11–13] conditions) and under pure thermal perturbation [14–17] have been extensively studied, the interplay between external shear and thermal activation in a general thermomechanical environment is known as a grand challenge [18] and remains largely unexplored until recently [19–22].

From a classic perspective, an applied shear stress would reduce the activation energy of an LSE whose resultant strain is compatible with the external loading. Such a picture is analogous to the migration of dislocations in crystals, where the Peierls valley in the potential energy landscape (PEL) is tilted by external shear [23]. In some studies, including the renowned free volume [24] and shear transformation zone [25,26] models, a linear stress dependence is assumed; while some other studies adopt a nonlinear parametrization [27,28]. According to such a classic picture, one should then expect a typical activation volume around several or tens of atomic volumes, in order to fit with experimental measurements [6,29,30]. On the other hand, however, atomistic modeling shows that LSEs' minimum energy pathways (MEPs) only change very weakly under applied shear stress [19], yielding a considerably smaller activation volume. Such a stark contrast suggests a lack of mechanistic understanding on how LSEs respond to external mechanical loading.

In the present study we investigate the ageing dynamics of a multiplicity of metastable glasses over broad thermomechanical conditions. By thoroughly sampling the energy landscape and scrutinizing the variations of MEPs under external shear, we demonstrate that the true reasons giving rise to the stress-accelerated ageing dynamics are the emergent fractality of the energy landscape and the consequently created tortuous but low-barrier excitations. These findings mark a departure from the conventional wisdom and pave the way to a new route to harness nonequilibrium disordered materials.

To examine the shear loading effects on thermally activated LSEs, we adopt a two-stage simulation protocol shown in Fig. 1. A widely used Cu-Zr metallic glass model [31] consisting of 2000 atoms is considered here because its dynamics under pure thermal scenario has been carefully studied [16,32–35], so that the present work can be better contextualized. Specifically, in stage I the samples are first equilibrated at 2000 K ($\sim 3T_g$) and then quenched to 0 K at controlled cooling rates. The focus is placed on the energetic evolution of the system's inherent structures (ISs), which are known as effective stability indicators of glasses [34,36–38]. As seen in Fig. 1(a), various cooling rates are employed across the typical span of MD timescales (0.01–10 Kps^{-1}) to create a multiplicity of glassy samples with different metastability, which are then subjected to the later shear loading analyses. At any given thermomechanical condition, we do 5 runs for each sample and use the averaged results to inspect the ageing relaxations. Although it is computationally demanding, one can expect to obtain a statistically more reliable understanding through such numerous samplings.

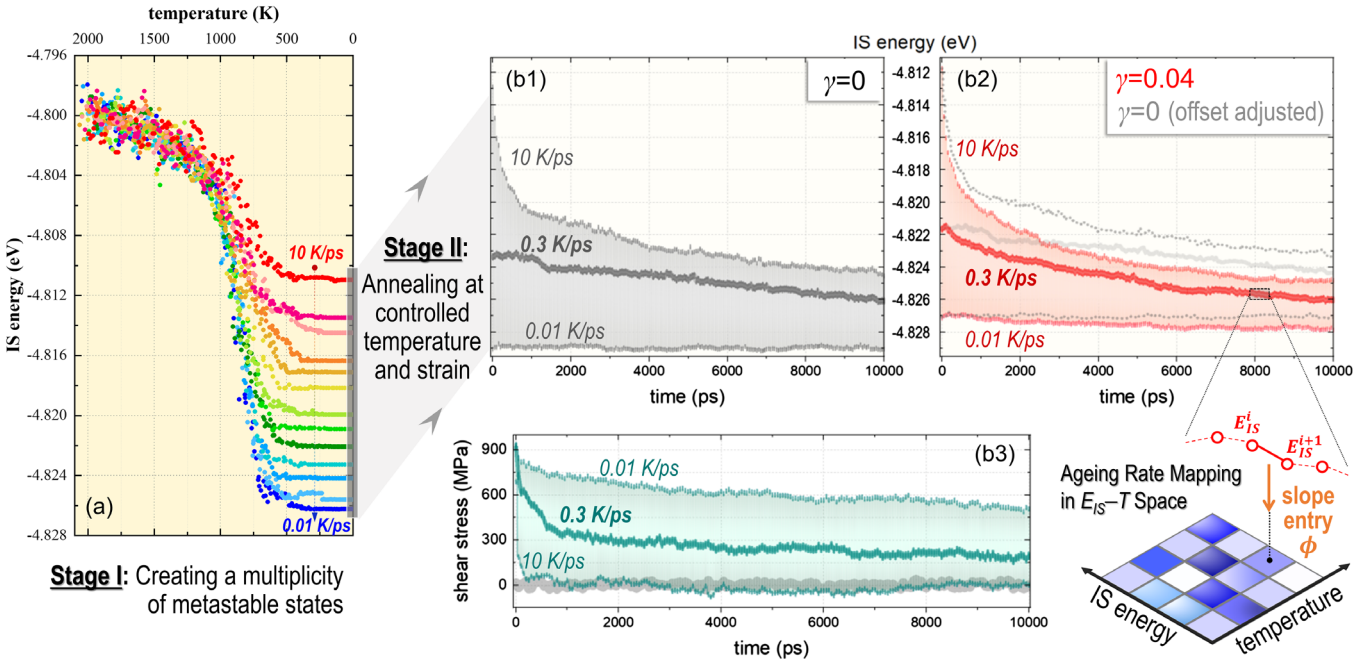

FIG. 1. (a) Glassy samples with various metastability are prepared by cooling at $0.01 \sim 10$ Kps^{-1}. (b1)–(b2) E_{IS} evolution at 600 K of 0.3 Kps^{-1} sample without (gray) and with (red) external shear. (b3) Stress evolution with (green) and without (gray) shear loading. Results at other temperatures are qualitatively similar (Supplemental Material, Fig. S1 [39]).

In stage II, controlled shear strains are imposed to the prepared samples, and the prestrained samples are then subjected to isothermal annealing at fixed temperatures for 10 ns, during which the IS energy evolution and shear stress relaxation are scrutinized. To restrict our scope to the interplay between external shear and thermal activation, the imposed strains are far below the plastic flow limit and the temperatures are controlled at intermediate range from 300 to 600 K ($0.4 \sim 0.8T_g$), so that the extreme scenarios like the high-stress athermal limit or high-temperature pure thermal limit can be avoided. By the same token, here we adopt a strain-control protocol rather than a strain rate-control or stress-control protocol because MD simulations under those controls might have a higher chance to develop dynamically increasing heterogeneities and drive the system to structural instabilities [11,43–46], which would obscure the scope of our study.

Figure 1(b1) shows the reference curves for the IS energy evolution of prepared samples at 600 K without external shear loading. To avoid the plot being too crowded, we only highlight the 0.3 Kps^{-1} sample's results, together with the upper and lower bounds of all samples. The profiles show a monotonic decreasing pattern, indicating a normal ageing behavior. The ageing rate is, however, nonuniform, and the curves' descending rates are evidently faster at a higher IS energy than that at a lower IS energy. This is because during ageing glasses evolve into deeper basins in the PEL and encounter with larger surrounding barriers, naturally slowing down the kinetics on the fly.

Figure 1(b2) shows the samples' annealing curves under an imposed shear strain of 0.04. The starting energy levels at $t = 0$ are higher than their counterparts in Fig. 1(b1) because of the shear-induced initial elastic strain energy. By adjusting such an initial offset one can clearly see that the samples' ageing rates become faster under external shear. The shear stresses [Fig. 1(b3)] also keep relaxing along with the annealing processes, and the stress relaxation is more drastic in a fast-quenched sample than in a slow-quenched sample. This is understandable because in a fast-quenched unstable sample the LSEs can be more easily activated, leading to more efficient energy dissipation and stress relaxation. However, it is challenging to quantify the stress effects because (i) glasses are inherently nonequilibrium systems, and their ageing rates are time and IS energy dependent even without external shear [Fig. 1(b1)]; (ii) in the presence of strain loading the shear stress itself also dynamically evolves [Fig. 1(b3)] and couples with the energetic evolution, making the characterization of stress effects further complicated. To address these challenges, here we construct the ageing rate mappings [35] in the temperature—IS energy (denoted as E_{IS}) parameter space and contrast the results of with and without loading, so that the entangled factors can be deconvoluted and unambiguously characterized.

As illustrated in Fig. 1, we calculate the slope between each pair of neighboring data points in a given isothermal annealing curve, $\Phi \equiv (E_{\mathrm{IS}}^{i+1} - E_{\mathrm{IS}}^{i})/\Delta t$, where Δt is set as 50 ps. The magnitude of calculated slope essentially

represents the system's ageing rate in the vicinity of that corresponding IS energy level and temperature. After mining all neighboring pairs in the annealing curves of all the prepared samples at various temperatures, in further integration with statistical averaging (Supplemental Material [39], Fig. S2), one can map out the ageing rate at a prescribed (E_{IS}, T) coordinate and color the pixel accordingly to its magnitude, $\Phi(E_{\mathrm{IS}}, T)$. By scanning such map horizontally or vertically, the effects of E_{IS} and T can thus be decoupled. For the shear loading scenario, the shear stress entries behind the pixels are also tractable from Fig. 1(b3). Therefore, by contrasting the same (E_{IS}, T)-coordinated pixels with and without loading, the stress effect can be explicitly characterized.

Figure 2(a1) shows the pixel-by-pixel ratios between the ageing rates with and without loading, defined as $f \equiv \Phi^{L}(E_{\mathrm{IS}}, T)/\Phi^{0}(E_{\mathrm{IS}}, T)$; while the average stress associated with each pixel in the shear loading scenario are displayed in Fig. 2(a2). The inset of Fig. 2(b) shows the plots between the ageing rate ratios and the stresses by vertically scanning Figs. 2(a1) and 2(a2) at various temperatures. A universal nonlinear dependence exhibits, and the ageing rate ratio becomes exceedingly larger at higher stress. The classic approach to characterize such an effect is to introduce stress-dependent activation energy [1,29]. Specifically, shear stress will tilt the system's underlying PEL and thus bias the MEPs' heights. A LSE's activation energy would become $\bar{E}_A^0 \mp \tau \cdot V_{\mathrm{act}}$, depending on whether the LSE's resultant strain is aligned (or against) with respect to external loading, where $\bar{E}_A^0$, τ, and V_{act} represents the effective activation energy without loading, shear stress, and activation volume, respectively. Therefore, in the presence of external stress the kinetic boost factor can be estimated as

$$f = \kappa^* \cdot \frac{\left(\exp\left[-\frac{\bar{E}_A^0 - \tau \cdot V_{\mathrm{act}}}{k_B T}\right] + \exp\left[-\frac{\bar{E}_A^0 + \tau \cdot V_{\mathrm{act}}}{k_B T}\right]\right)/2}{\exp\left[-\frac{\bar{E}_A^0}{k_B T}\right]} = \kappa^* \cdot \cosh\left(\tau \cdot \frac{V_{\mathrm{act}}}{k_B T}\right), \quad (1)$$

where a numerical prefactor κ^* could exist because the attempt frequency may not strictly be a constant [6,24,47,48]. Note that while individual MD simulation is known for its intrinsic timescale limitation, by taking the ratio of the kinetics in two parallel sets of simulations (with and without loading) such timescale limitation should have been canceled out, and what obtained in Fig. 2 is a clean net effect of stress-induced kinetic boosting factor.

It is evident in Fig. 2(b) that all the data points indeed follow such a hyperbolic cosine relationship, yielding a fitted activation volume around $V_{\mathrm{act}} \sim 60 \pm 22.92$ Å^3. This value is in line with experiments [6,29,30], which reportedly range from 60 to several hundred Å^3, depending on the compositions and measurement techniques. It is worth realizing that some previously reported large activation volumes are attributed to the structural heterogeneity (e.g., shear banding) formed during measurements [30,49]. By contrast, the strain-control protocol employed in the present study ensures that no large-scale structural heterogeneity would appear. Therefore, our hereby obtained results are reasonable.

To acquire a fundamental understanding on how individual LSEs' activation energy are altered by external shear, here we seek to directly probe the system's underlying PEL, because LSEs are known to correspond to elementary hopping between neighboring local minima in PEL [50–52]. Activation relaxation technique (ART) [53–55] is employed to identify both the surrounding saddle states to a zero-load sample and their connecting neighboring local minima. The hereby obtained information are then fed into the nudged elastic band algorithm [56–58] to accurately map out the entire MEPs. The effects of external shear are investigated by further rendering the obtained MEPs to controlled shear strains. It is found that, while a small fraction of MEPs no longer has correspondences after shear loading due to the qualitative changes of PEL's topology (details in Supplemental Material [39], Fig. S3), the majority of existing MEPs still persist and only exhibit quantitative changes. As a representative example, Fig. 3(a) shows the shear-induced variations of MEPs in a sample prepared at 0.02 Kps^{-1}. The results are broadly distributed both above and below zero, indicating a LSE's activation barrier can be either reduced or increased by external loading. It is also noticed a higher imposed strain would increase the scatteredness of the results. Importantly, the barrier variations are not symmetric and slightly skewed towards the upper half plane, meaning statistically the LSEs' activation barriers become smaller

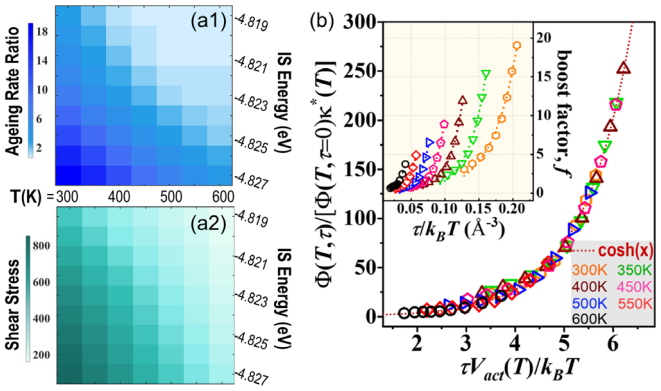

FIG. 2. (a1)–(a2) Pixel maps of ageing rate ratio and stress in $E_{\mathrm{IS}} - T$ space. (b) Normalized correlation between boost factor and stress at various T. They all follow Eq. (1), yielding a fitted activation volume around 60 Å^3. Inset shows the original scattered plots by scanning (a1)–(a2).

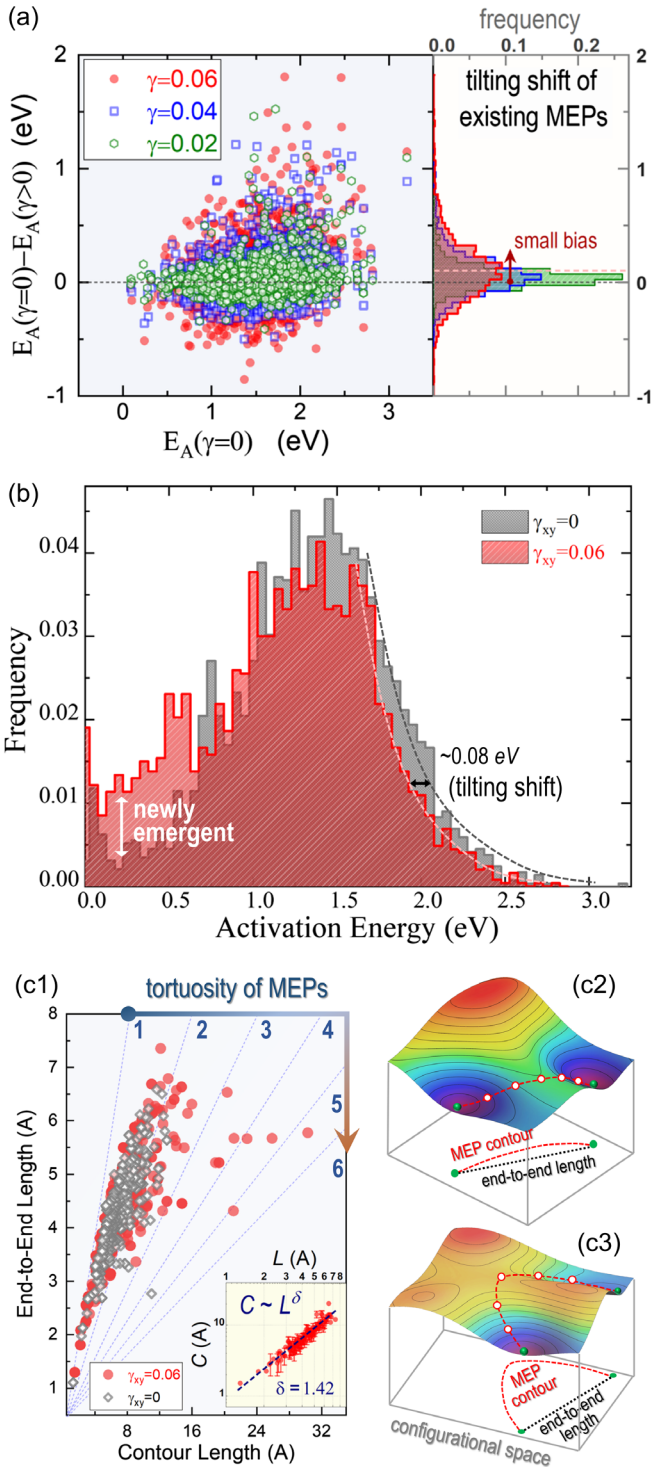

FIG. 3. (a) Weak E_A changes due to shear-induced tilting of existing MEPs. (b) E_A spectra at $\gamma_{xy} = 0.06$ and zero load. (c1) Correlation between end-to-end length and contour length of MEPs and corresponding tortuosity. Fractal dimension analysis in the inset plot yields a value of 1.42. (c2)–(c3) Schematics of MEPs with small and large tortuosity on simplified 3D landscape.

under shear. Characterizing the histogram's peak shift with respect to strain in the right panel allows one to directly derive the activation volume, which yields a surprisingly small value around 10 A^3. Such a small V_{act} cannot possibly explain the huge kinetic difference in Fig. 2. The remarkable discrepancy herein suggests that there must be other alternative mechanisms, in addition to the classic PEL tilting picture, that should account for the stress-accelerated dynamics.

In Fig. 3(b) we obtain the full activation energy spectrum at $\gamma_{xy} = 0.06$ by ART and contrast it to the original zero-load E_A spectrum. It is observed that the main peak is slightly shifted towards left (by ~0.08 eV) under shear, and such a picture is consistent with the above tilting analyses on the existing MEPs. On the other hand, remarkably, numerous low-barrier events less than 1 eV are captured. Given its significant fraction, such a low-E_A mode cannot come from the simple bias of the PEL and instead must represent some newly emergent excitations created by the external loading. Consequently, these newly emergent LSEs provide natural explanations to the stress-accelerated activities that cannot be otherwise justified by the conventional PEL tilting picture.

To further probe the nature of these shear-induced excitations, we examine the topologies of their corresponding MEPs. Figure 3(c1) shows the correlations between the contour length (C) and end-to-end length (L) for the MEPs with $E_A < 1$ eV. Almost all the data points in the zero-load sample exhibit small slope around $1 \sim 2$, indicating relatively straight MEPs in the PEL as illustrated in Fig. 3(c2). However, the sheared sample exhibits a more scattered distribution with some large C/L ratios up to 5, indicating very tortuous MEPs illustrated in Fig. 3(c3). An increased MEP tortuosity usually reflects a more fractal feature of the hyperdimensional configuration space, the results herein therefore suggest that external loading would qualitatively change glasses' PEL and make it statistically more fractal. A more quantitative analysis in the inset of Fig. 3(c1) shows a scaling of $C \sim L^{\delta}$, with the fractal dimension $\delta \sim 1.42$. Coincidently, this number is close to the fractal dimension (~1.47) for the superdiffusive Levy walk in colloidal glasses [59], which may imply certain universal PEL scaling in general disordered systems warranting future research.

In addition to the marked topological changes of PEL, the dynamics of LSEs with different C/L ratios are also studied. Here we characterize individual atoms' mobility by the hopping indicator p^i_{hop}, a time-space correlation function widely adopted to examine particles' activity in disordered materials [60–62]. The atoms in the top-5% and medium-5% hopping windows are visualized in Figs. 4(a1) and 4(a2). We then color the particles according to the C/L ratios of LSEs that those atoms participate in. Note that in amorphous materials the same atom can involve multiple LSEs [25,26,63], and in that case the largest C/L ratio is considered. Should there exist no correlation between p^i_{hop} and C/L ratio, then similar color distributions in Figs. 4(a3) and 4(a4) are expected.

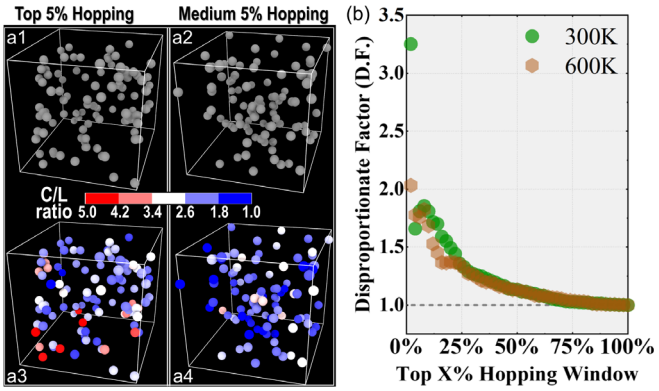

FIG. 4. (a1)–(a2) The atoms in top 5% and medium 5% mobility windows. (a3)–(a4) The same atoms colored by C/L-ratio of corresponding LSEs. (b) Variation of $D.F.(X\%)$ function at various percentile of top mobility atoms windows.

However, the clear contrast suggests that the top p^i_{hop} window contains a disproportionate high fraction of atoms involved in the large C/L ratio LSEs. To quantify such a disproportionate factor, we define a $D.F.(X\%)$ function:

$$D.F.(X\%) \equiv \frac{f(i \in \{\mathrm{top}X\% \frac{C}{L}\mathrm{ratio}\} | i \in \{\mathrm{top}X\% p^i_{\mathrm{hop}}\})}{O(i \in \{\mathrm{top}X\% \frac{C}{L}\mathrm{ratio}\})}, \tag{2}$$

where the numerator represents the fraction of particles involved in the top $X\%$ C/L *ratio* LSEs among those atoms within the top $X\%$ hopping window, while the denominator means the occupation of atoms involved in the top $X\%$ C/L-*ratio* LSEs out of the whole sample. Since the amount of atoms engaged in a LSE is not a predetermined constant number [16,29,64], a normalization factor $O(X\%)$ is therefore needed in the denominator.

Following such a definition, the value of $D.F.$ would be 1 either (i) when there is no correlation between p^i_{hop} and C/L ratio, or, (ii) when the analysis window expands to the entire sample, i.e., $\mathbf{X}\% = 100\%$. As shown in Fig. 4(b), the disproportionate factor exhibits a clear monotonic descending pattern and eventually converges to 1 at wider window. It means the large C/L-*ratio* LSEs would contribute more effectively to the activity of atoms, which lends further credence to the significant stress-accelerated relaxations seen in Figs. 1–2. Markedly, the hereby obtained highest $D.F.$ value around 3 in Fig. 4(b) is consistent with a recent study on the creep of amorphous solids [46], where it was reported that the atoms' mobility can be boosted by a factor of 3 at high stress compared with the case at low stress.

To further examine the validity of the findings above at more realistic conditions, in the Supplemental Material [39] we prepare an ultrastable sample comparable with experiment by employing advanced swap algorithm [65–68] and sub-T_g annealing simulation [69,70]. It is found the stress effect remains the same (Fig. S4 [39]). We believe the remarkable stress impact on PEL, namely the enhanced fractality and the creation of new low-E_A mode, can shed light on understanding the glass dynamics and plasticity under external stimuli. For example, in addition to the widely recognized α and β relaxations, recent dynamic mechanical analysis experiments [71–73] reveal a third relaxation mode at smaller energy scale overlapping with the hereby obtained newly emergent excitations in Fig. 3(b). Therefore, the present study may provide rationale for these phenomena from a fundamental level. In further considering many reported similarities between glasses and other important systems (e.g., nanocrystals [62,74,75], active matters [76]), there is a reason to expect the new findings herein can be broadly applicable.

To summarize, in stark contrast to the empirical PEL tilting picture, we have demonstrated the origin of activation volume in amorphous solids should be attributed to the enhanced tortuosity of MEPs in a more fractal PEL promoted by mechanical loading. Fractal features of PEL in glassy materials have drawn significant attention recently [59,77–79] in terms of their connections to the critical phenomena such as jamming and rheology, and our study provides further evidence in the same vein. As a final remark, activation volume is the key concept to bridge a system's physical responses to external stimuli. It is broadly applicable to essentially any condensed matters, including crystals [80,81], amorphous solids [6,47], and polymers [82–84]. Therefore, the present study might shed a new perspective on the control of glassy materials and thus represent a rich avenue for future inquiry.

This work was funded by NSF DMR-2104136. The authors thank J. Hwang and Y. Wang for insightful comments and discussions.

*Corresponding author.
fanyue@umich.edu

[1] A. S. Argon, Plastic deformation in metallic glasses, Acta Metall. **27**, 47 (1979).
[2] M. L. Falk and J. S. Langer, Dynamics of viscoplastic deformation in amorphous solids, Phys. Rev. E **57**, 7192 (1998).
[3] C. A. Schuh and A. C. Lund, Atomistic basis for the plastic yield criterion of metallic glass, Nat. Mater. **2**, 449 (2003).
[4] S. Swayamjyoti, J. F. Löffler, and P. M. Derlet, Local structural excitations in model glasses, Phys. Rev. B **89**, 224201 (2014).
[5] Y. Wu, H. H. Wu, X. D. Hui, G. L. Chen, and Z. P. Lu, Effects of drawing on the tensile fracture strength and its reliability of small-sized metallic glasses, Acta Mater. **58**, 2564 (2010).
[6] M. Heggen, F. Spaepen, and M. Feuerbacher, Creation and annihilation of free volume during homogeneous flow of a metallic glass, J. Appl. Phys. **97**, 033506 (2005).

[7] H. B. Yu, K. Samwer, Y. Wu, and W. H. Wang, Correlation between β Relaxation and Self-Diffusion of the Smallest Constituting Atoms in Metallic Glasses, Phys. Rev. Lett. **109**, 095508 (2012).

[8] S. V. Khonik, A. V. Granato, D. M. Joncich, A. Pompe, and V. A. Khonik, Evidence of Distributed Interstitialcy-Like Relaxation of the Shear Modulus due to Structural Relaxation of Metallic Glasses, Phys. Rev. Lett. **100**, 065501 (2008).

[9] C. E. Maloney and A. Lemaître, Amorphous systems in athermal, quasistatic shear, Phys. Rev. E **74**, 016118 (2006).

[10] P. Leishangthem, A. D. S. Parmar, and S. Sastry, The yielding transition in amorphous solids under oscillatory shear deformation, Nat. Commun. **8**, 14653 (2017).

[11] Y. Q. Cheng and E. Ma, Intrinsic shear strength of metallic glass, Acta Mater. **59**, 1800 (2011).

[12] D. Şopu, Y. Ritter, H. Gleiter, and K. Albe, Deformation behavior of bulk and nanostructured metallic glasses studied via molecular dynamics simulations, Phys. Rev. B **83**, 100202(R) (2011).

[13] J. S. Langer and T. Egami, Glass dynamics at high strain rates, Phys. Rev. E **86**, 011502 (2012).

[14] Y. Q. Cheng and E. Ma, Configurational dependence of elastic modulus of metallic glass, Phys. Rev. B **80**, 064104 (2009).

[15] J. Ding, Y.-Q. Cheng, and E. Ma, Full icosahedra dominate local order in $Cu_{64}Zr_{34}$ metallic glass and supercooled liquid, Acta Mater. **69**, 343 (2014).

[16] Y. Fan, T. Iwashita, and T. Egami, How thermally activated deformation starts in metallic glass, Nat. Commun. **5**, 5083 (2014).

[17] Y. Fan, T. Iwashita, and T. Egami, Crossover from Localized to Cascade Relaxations in Metallic Glasses, Phys. Rev. Lett. **115**, 045501 (2015).

[18] D. Rodney, A. Tanguy, and D. Vandembroucq, Modeling the mechanics of amorphous solids at different length scale and time scale, Model. Simul. Mater. Sci. Eng. **19**, 083001 (2011).

[19] S. Swayamjyoti, J. F. Löffler, and P. M. Derlet, Local structural excitations in model glass systems under applied load, Phys. Rev. B **93**, 144202 (2016).

[20] S. Küchemann, C. Liu, E. M. Dufresne, J. Shin, and R. Maaß, Shear banding leads to accelerated aging dynamics in a metallic glass, Phys. Rev. B **97**, 014204 (2018).

[21] A. Das, P. Kagebein, S. Küchemann, and R. Maaß, Temperature rise from fracture in a Zr-based metallic glass, Appl. Phys. Lett. **112**, 261905 (2018).

[22] A. Das, P. M. Derlet, C. Liu, E. M. Dufresne, and R. Maaß, Stress breaks universal aging behavior in a metallic glass, Nat. Commun. **10**, 5006 (2019).

[23] D. Rodney and L. Proville, Stress-dependent Peierls potential: Influence on kink-pair activation, Phys. Rev. B **79**, 094108 (2009).

[24] F. Spaepen, A microscopic mechanism for steady state inhomogeneous flow in metallic glasses, Acta Metall. **25**, 407 (1977).

[25] L. Li, E. R. Homer, and C. A. Schuh, Shear transformation zone dynamics model for metallic glasses incorporating free volume as a state variable, Acta Mater. **61**, 3347 (2013).

[26] P. Zhao, J. Li, and Y. Wang, Heterogeneously randomized STZ model of metallic glasses: Softening and extreme value statistics during deformation, Int. J. Plast. **40**, 1 (2013).

[27] J. Chattoraj, C. Caroli, and A. Lemaître, Universal Additive Effect of Temperature on the Rheology of Amorphous Solids, Phys. Rev. Lett. **105**, 266001 (2010).

[28] W. L. Johnson and K. Samwer, A Universal Criterion for Plastic Yielding of Metallic Glasses with a $(T/T_g)^{2/3}$ Temperature Dependence, Phys. Rev. Lett. **95**, 195501 (2005).

[29] C. A. Schuh, T. C. Hufnagel, and U. Ramamurty, Mechanical behavior of amorphous alloys, Acta Mater. **55**, 4067 (2007).

[30] M. Ghidelli, S. Gravier, J. J. Blandin, P. Djemia, F. Mompiou, G. Abadias, J. P. Raskin, and T. Pardoen, Extrinsic mechanical size effects in thin ZrNi metallic glass films, Acta Mater. **90**, 232 (2015).

[31] Y. Q. Cheng, E. Ma, and H. W. Sheng, Atomic Level Structure in Multicomponent Bulk Metallic Glass, Phys. Rev. Lett. **102**, 245501 (2009).

[32] J. Ding, S. Patinet, M. L. Falk, Y. Cheng, and E. Ma, Soft spots and their structural signature in a metallic glass, Proc. Natl. Acad. Sci. U.S.A. **111**, 14052 (2014).

[33] J. Ding, Y.-Q. Cheng, H. Sheng, M. Asta, R. O. Ritchie, and E. Ma, Universal structural parameter to quantitatively predict metallic glass properties, Nat. Commun. **7**, 13733 (2016).

[34] Y. Fan, T. Iwashita, and T. Egami, Energy landscape-driven non-equilibrium evolution of inherent structure in disordered material, Nat. Commun. **8**, 15417 (2017).

[35] C. Liu, X. Yan, P. Sharma, and Y. Fan, Unraveling the non-monotonic ageing of metallic glasses in the metastability-temperature space, Comput. Mater. Sci. **172**, 109347 (2020).

[36] A. Heuer, Exploring the potential energy landscape of glass-forming systems: From inherent structures via metabasins to macroscopic transport, J. Phys. Condens. Matter **20**, 373101 (2008).

[37] C. Rehwald, N. Gnan, A. Heuer, T. Schrøder, J. C. Dyre, and G. Diezemann, Aging effects manifested in the potential-energy landscape of a model glass former, Phys. Rev. E **82**, 021503 (2010).

[38] J. Helfferich, I. Lyubimov, D. Reid, and J. J. de Pablo, Inherent structure energy is a good indicator of molecular mobility in glasses, Soft Matter **12**, 5898 (2016).

[39] See Supplemental Material at http://link.aps.org/supplemental/10.1103/PhysRevLett.127.215502 for the system's ageing dynamics at other thermo-mechanical conditions and more details of data analyses, which includes Refs. [40–42].

[40] Y. Huang, J. Shen, Y. Sun, J. Sun, and J. J. J. Chen, High temperature deformation behaviors of $Ti_{40}Zr_{25}Ni_3Cu_{12}Be_{20}$ bulk metallic glass, J. Alloys Compd. **504**, S82 (2010).

[41] Y. Chen and J. Qiao, Correlation between high temperature deformation and β relaxation in LaCe-based metallic glass, Materials **13**, 833 (2020).

[42] K. Vollmayr, W. Kob, and K. Binder, How do the properties of a glass depend on the cooling rate? A computer

simulation study of a Lennard-Jones system, J. Chem. Phys. **105**, 4714 (1996).
[43] T. C. Hufnagel, C. A. Schuh, and M. L. Falk, Deformation of metallic glasses: Recent developments in theory, simulations, and experiments, Acta Mater. **109**, 375 (2016).
[44] S. Ogata, F. Shimizu, J. Li, M. Wakeda, and Y. Shibutani, Atomistic simulation of shear localization in Cu–Zr bulk metallic glass, Intermetallics **14**, 1033 (2006).
[45] Y. Shi and M. L. Falk, Atomic-scale simulations of strain localization in three-dimensional model amorphous solids, Phys. Rev. B **73**, 214201 (2006).
[46] P. Cao, M. P. Short, and S. Yip, Understanding the mechanisms of amorphous creep through molecular simulation, Proc. Natl. Acad. Sci. U.S.A. **114**, 13631 (2017).
[47] M. Bletry, P. Guyot, J. J. Blandin, and J. L. Soubeyroux, Free volume model: High-temperature deformation of a Zr-based bulk metallic glass, Acta Mater. **54**, 1257 (2006).
[48] F. Spaepen, Homogeneous flow of metallic glasses: A free volume perspective, Scr. Mater. **54**, 363 (2006).
[49] L. S. Huo, J. F. Zeng, W. H. Wang, C. T. Liu, and Y. Yang, The dependence of shear modulus on dynamic relaxation and evolution of local structural heterogeneity in a metallic glass, Acta Mater. **61**, 4329 (2013).
[50] F. H. Stillinger, A topographic view of supercooled liquids and glass formation, Science **267**, 1935 (1995).
[51] S. Sastry, P. G. Debenedetti, and F. H. Stillinger, Signatures of distinct dynamical regimes in the energy landscape of a glass-forming liquid, Nature (London) **393**, 554 (1998).
[52] P. G. Debenedetti and F. H. Stillinger, Supercooled liquids and the glass transition, Nature (London) **410**, 259 (2001).
[53] G. T. Barkema and N. Mousseau, Event-Based Relaxation of Continuous Disordered Systems, Phys. Rev. Lett. **77**, 4358 (1996).
[54] N. Mousseau and G. T. Barkema, Traveling through potential energy landscapes of disordered materials: The activation-relaxation technique, Phys. Rev. E **57**, 2419 (1998).
[55] E. Cancès, F. Legoll, M. C. Marinica, K. Minoukadeh, and F. Willaime, Some improvements of the activation-relaxation technique method for finding transition pathways on potential energy surfaces, J. Chem. Phys. **130**, 114711 (2009).
[56] G. Henkelman, B. P. Uberuaga, and H. Jónsson, A climbing image nudged elastic band method for finding saddle points and minimum energy paths, J. Chem. Phys. **113**, 9901 (2000).
[57] A. Nakano, A space–time-ensemble parallel nudged elastic band algorithm for molecular kinetics simulation, Comput. Phys. Commun. **178**, 280 (2008).
[58] G. Mills, H. Jónsson, and G. K. Schenter, Reversible work transition state theory: Application to dissociative adsorption of hydrogen, Surf. Sci. **324**, 305 (1995).
[59] H. J. Hwang, R. A. Riggleman, and J. C. Crocker, Understanding soft glassy materials using an energy landscape approach, Nat. Mater. **15**, 1031 (2016).
[60] A. S. Keys, L. O. Hedges, J. P. Garrahan, S. C. Glotzer, and D. Chandler, Excitations Are Localized and Relaxation Is Hierarchical in Glass-Forming Liquids, Phys. Rev. X **1**, 021013 (2011).
[61] S. S. Schoenholz, E. D. Cubuk, D. M. Sussman, E. Kaxiras, and A. J. Liu, A structural approach to relaxation in glassy liquids, Nat. Phys. **12**, 469 (2016).
[62] T. A. Sharp, S. L. Thomas, E. D. Cubuk, S. S. Schoenholz, D. J. Srolovitz, and A. J. Liu, Machine learning determination of atomic dynamics at grain boundaries, Proc. Natl. Acad. Sci. U.S.A. **115**, 10943 (2018).
[63] C. Liu, P. Guan, and Y. Fan, Correlating defects density in metallic glasses with the distribution of inherent structures in potential energy landscape, Acta Mater. **161**, 295 (2018).
[64] J. D. Ju and M. Atzmon, A comprehensive atomistic analysis of the experimental dynamic-mechanical response of a metallic glass, Acta Mater. **74**, 183 (2014).
[65] D. Khomenko, C. Scalliet, L. Berthier, D. R. Reichman, and F. Zamponi, Depletion of Two-Level Systems in Ultrastable Computer-Generated Glasses, Phys. Rev. Lett. **124**, 225901 (2020).
[66] D. Khomenko, D. R. Reichman, and F. Zamponi, Relationship between two-level systems and quasilocalized normal modes in glasses, Phys. Rev. Mater. **5**, 055602 (2021).
[67] W. Ji, T. W. J. de Geus, E. Agoritsas, and M. Wyart, Geometry of hopping processes and local excitations in glasses, arXiv:2106.13153.
[68] A. Ninarello, L. Berthier, and D. Coslovich, Models and Algorithms for the Next Generation of Glass Transition Studies, Phys. Rev. X **7**, 021039 (2017).
[69] F. Zhang, M. I. Mendelev, Y. Zhang, C.-Z. Wang, M. J. Kramer, and K.-M. Ho, Effects of sub-Tg annealing on $Cu_{64.5}Zr_{35.5}$ glasses: A molecular dynamics study, Appl. Phys. Lett. **104**, 061905 (2014).
[70] Y. Wang and Y. Fan, Incident velocity induced nonmonotonic aging of vapor-deposited polymer glasses, J. Phys. Chem. B **124**, 5740 (2020).
[71] Q. Wang, S. T. Zhang, Y. Yang, Y. D. Dong, C. T. Liu, and J. Lu, Unusual fast secondary relaxation in metallic glass, Nat. Commun. **6**, 7876 (2015).
[72] Q. Wang, J. J. Liu, Y. F. Ye, T. T. Liu, S. Wang, C. T. Liu, J. Lu, and Y. Yang, Universal secondary relaxation and unusual brittle-to-ductile transition in metallic glasses, Mater. Today **20**, 293 (2017).
[73] S. Küchemann and R. Maaß, Gamma relaxation in bulk metallic glasses, Scr. Mater. **137**, 5 (2017).
[74] H. Zhang, D. J. Srolovitz, J. F. Douglas, and J. A. Warren, Grain boundaries exhibit the dynamics of glass-forming liquids, Proc. Natl. Acad. Sci. U.S.A. **106**, 7735 (2009).
[75] Z. Bai, G. H. Balbus, D. S. Gianola, and Y. Fan, Mapping the kinetic evolution of metastable grain boundaries under non-equilibrium processing, Acta Mater. **200**, 328 (2020).
[76] T. E. Angelini, E. Hannezo, X. Trepat, M. Marquez, J. J. Fredberg, and D. A. Weitz, Glass-like dynamics of collective cell migration, Proc. Natl. Acad. Sci. U.S.A. **108**, 4714 (2011).
[77] C. P. Massen and J. P. K. Doye, Power-law distributions for the areas of the basins of attraction on a potential energy landscape, Phys. Rev. E **75**, 037101 (2007).
[78] P. Charbonneau, J. Kurchan, G. Parisi, P. Urbani, and F. Zamponi, Fractal free energy landscapes in structural glasses, Nat. Commun. **5**, 3725 (2014).

[79] P. Cao, M. P. Short, and S. Yip, Potential energy landscape activations governing plastic flows in glass rheology, Proc. Natl. Acad. Sci. U.S.A. **116**, 18790 (2019).

[80] R. J. Asaro and S. Suresh, Mechanistic models for the activation volume and rate sensitivity in metals with nano-crystalline grains and nano-scale twins, Acta Mater. **53**, 3369 (2005).

[81] Z. Bai and Y. Fan, Abnormal Strain Rate Sensitivity Driven by a Unit Dislocation-Obstacle Interaction in BCC Fe, Phys. Rev. Lett. **120**, 125504 (2018).

[82] J. Ho, L. Govaert, and M. Utz, Plastic deformation of glassy polymers: Correlation between shear activation volume and entanglement density, Macromolecules **36**, 7398 (2003).

[83] W.-S. Xu, J. F. Douglas, W. Xia, and X. Xu, Understanding activation volume in glass-forming polymer melts via generalized entropy theory, Macromolecules **53**, 7239 (2020).

[84] M. Wendlandt, T. A. Tervoort, and U. W. Suter, Non-linear, rate-dependent strain-hardening behavior of polymer glasses, Polymer **46**, 11786 (2005).